

## Analyzing the Influence of Global Ionospheric Scintillation on GPS PPP during the Geomagnetic Storm of 26-28 February 2023

Shuanglei Cui<sup>1,2</sup>, Xueli Zhang<sup>1</sup>, Dongsheng Zhao<sup>✉1,2</sup>, Wei Ban<sup>3</sup>, Qianxin Wang<sup>1</sup>,  
Craig M. Hancock<sup>4</sup> and Kefei Zhang<sup>1</sup>

- 1) Observation and Research Station of Jiangsu Jiawang Resource Exhausted Mining Area Land Restoration and Ecological Succession, Ministry of Education, China University of Mining and Technology, Xuzhou, China
- 2) State Key Laboratory of Geo-Information Engineering Xi'an 710054.China
- 3) Chinese Antarctic Center of Surveying and Mapping, Wuhan University, Wuhan, Hubei, China
- 4) School of Architecture, Building and Civil Engineering, Loughborough University, United Kingdom

✉ Corresponding author, [dszhao@cumt.edu.cn](mailto:dszhao@cumt.edu.cn)

**Abstract:** This study examines the influence of ionospheric scintillation on GPS Precise Point Positioning (PPP) during a geomagnetic storm event that took place on February 26-28th, 2023. The analysis utilizes data from global IGS stations, as well as stations in Alaska, Canada, and Hong Kong. Findings indicate that geomagnetic storms can trigger ionospheric scintillation, leading to disruptions in GPS positioning accuracy. However, it is important to note that not all instances of ionospheric scintillation are solely attributed to geomagnetic storms; they can also arise from the interaction between charged particles and the ionosphere. During geomagnetic storms, ionospheric scintillation occurs first at high latitudes and spreads to lower latitudes, and the overall impact is most severe at high latitudes, where most of the affected stations have a positioning error of more than 0.5 m, while most of the stations at the equator have a positioning error of 0.15-0.5 m. The impact on positioning accuracy is most severe before and after the peak of geomagnetic storms. The impact on positioning accuracy was most severe before and after the peaks of geomagnetic storms, with PPP 3DRMS exceeding 0.5 m at more than 80% of the stations in the high-latitude regions of North America, Europe, Hong Kong, and New Caledonia in eastern Australia.

**Keywords:** GPS, Geomagnetic storms, Precise Point Positioning, Ionospheric scintillation

### 1. Introduction

Geomagnetic storms, which follow solar activities like solar flares, coronal mass ejections, and high-speed solar wind streams, are significant disturbances in the global space environment. These storms occur when high-speed plasma clouds, generated by solar activity, reach the vicinity of Earth

a few days later, causing disruptions in the Earth's magnetic field. This phenomenon is known as a geomagnetic storm (Gonzalez et al., 1994). Geomagnetic storms have a profound impact on GPS PPP by amplifying and varying ionospheric delays in GPS phase and code data. This, in turn, affects high-precision GPS relative positioning (Odijk, 2001). In low-to-mid latitudes, geomagnetic storms can even cause disruptions in total electron content (TEC) and result in satellite signal loss (Astafyeva et al., 2014).

Ionospheric scintillation is closely linked to disturbances in the geomagnetic field, particularly in high-latitude regions (Jiao & Morton, 2015). Ionospheric scintillation refers to random fluctuations in the amplitude and phase of radio signals as they pass through ionospheric plasma density irregularities (Basu & Groves, 2002). Various factors influence ionospheric scintillation, including the intensity of geomagnetic storms, storm onset time, local time, season, day-night variations, and latitude (Fuller-Rowell et al., 1994; Nava et al., 2016; Mansilla, 2019; Zhao et al., 2021). It is most commonly observed during the post-sunset hours in equatorial and polar regions during periods of strong solar activity (Li et al., 2010; Béniguel et al., 2011; Marques et al., 2016; Veellil et al., 2020). Luo et al. (2018) conducted a comparative study between the ROTI index calculated from the Hong Kong Satellite Positioning Reference Network station and the S4 and  $\sigma\phi$  scintillation indices collected by an Ionospheric Scintillation Monitoring Receiver (ISMR), confirming that the ROTI can be used as a scintillation detection index instead of the S4 and  $\sigma\phi$ . Juan et al. (2018) proposed a strong correlation between the ionospheric perturbations and the along-arc TEC rate AATR index, and then Wilken et al. (2018) proposed a new DIXSG index that can correctly characterize the temporal and spatial variations of the ionosphere at small and medium

scales, and the DIXSG index has a strong correlation with the Dst index, and thus is suitable for indicating geomagnetic storm events.

During periods of scintillation, the penetration of magnetospheric electric fields into the ionosphere causes fluctuations in TEC, adversely affecting navigation systems (Basu et al., 2001). Ionospheric scintillation interferes with positioning accuracy in several ways, primarily due to range errors and satellite

signal loss (cycle slips) (Basu & Groves, 2002; Conker et al., 2003; Zhang et al., 2014; Zhao et al., 2019; Luo et al., 2022). Bergeot et al. (2011) investigated the effects of GPS positioning during the Halloween storm of 2003 and identified TEC and magnetic field perturbations as contributors to degraded kinematic PPP caused by second-order signal delays. Yang et al. (2020) analyzed ionospheric disturbances resulting from geomagnetic storms during the Saint Patrick's Day storm in 2015. They utilized dual-frequency carrier observations from over 5500 GNSS stations worldwide to derive kinematic PPP solutions, revealing more severe impacts in high-latitude regions and variations in PPP degradation based on different types of ionospheric disturbances in lower latitudes. Luo et al. (2018) conducted kinematic

PPP using the BeiDou Navigation Satellite System (BDS) during scintillation periods and found that both horizontal and vertical positioning RMS errors exceed 0.5m.

This study aims to analyze the influence of ionospheric scintillation induced by geomagnetic storms on kinematic PPP solutions using GPS. The DIXSG index will be utilized to characterize the geomagnetic storm event that occurred from February 26-28, 2023, while the ROTI index will provide insights into ionospheric scintillation.

## 2. Data and Method

### 2.1 GPS data

In this paper, global IGS station and Alaska, CHAIN, and Hong Kong regional station data from February 26 to 28, 2023 are used, totaling 313 stations, of which 240 are IGS stations, 32 are Alaska stations, 23 are CHAIN stations, and 18 are Hong Kong stations. The sampling rate of the station data is 30s, and only GPS signals are used in the kinematic PPP solving. Figure 1 shows the geographical distribution of all the stations used in this study.

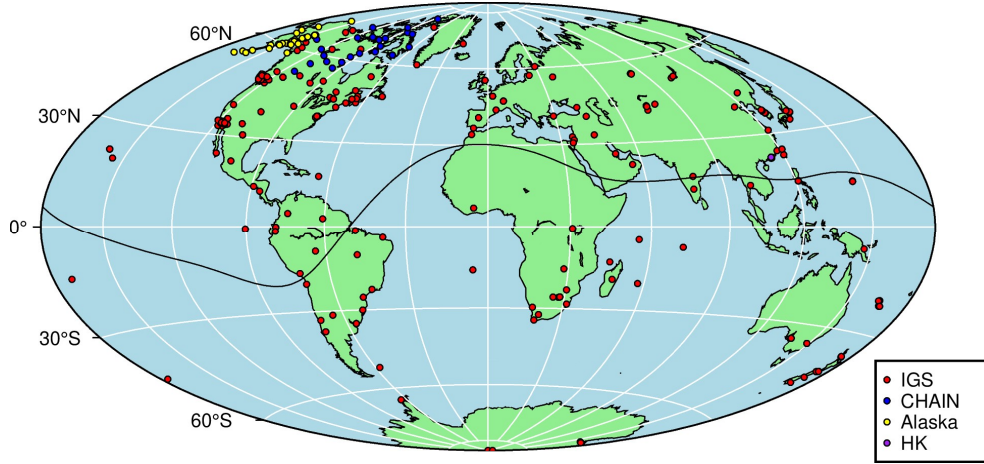


**Figure 1.** The geographical distribution of the stations. The solid black line indicates the magnetic equator. IGS stations are represented by the color red, Alaska stations by yellow, CHAIN stations by blue, and Hong Kong Observatory stations by purple.

### 2.2 Disturbance Ionosphere Index Spatial Gradient (DIXSG)

The Disturbance Ionosphere Index Spatial Gradient (DIXSG) is derived from the calculation of the Disturbance Ionosphere Index (DIX) using differential GNSS carrier phase observations, building upon the research conducted by Wilken et al. (2018). Initially, the gradient variation of Slant Total Electron Content (STEC), which is weighted by the elevation angle over time, is computed as follows:

$$cROT_m^k = \frac{|\Delta STEC_m^k|}{|\Delta t \cdot \Delta s|} \quad (1)$$

where  $\Delta STEC$  denotes the change in STEC between two consecutive observation arcs at a given epoch.  $k$  represents the satellites,  $m$  represents the receivers, and  $\Delta s$  represents the distance between the Ionospheric Pierce Points (IPPs) at a predetermined assumed ionospheric height within a specific time interval  $\Delta t$ . This distance parameter helps mitigate interference caused by satellite elevation angles. Subsequently, the DIXSG is determined under a specified sensitivity level condition:

$$DIXSG(cROT_{(level)})_{i,j}^k = \left( \frac{|cROT_m^k - cROT_n^k|}{cROT_{level}} \right)^3 \left( \frac{d}{D} \right)^{-1} \quad (2)$$

where  $cROT_{(level)}$  represents the sensitivity level,  $n$  represents the receivers,  $d$  represents the distance between satellite  $k$  and the corresponding IPPs for receivers  $m$  and  $n$ , and  $D$  represents the maximum permissible distance within the receiver observation network, which is typically set to 1000 km. The user has the flexibility to choose the size and number of sensitivity levels. To simplify the DIXSG under different sensitivity levels, the calculated DIXSG values are reassigned as follows:

$$DIXSG(cROT_{(level)})_{m,n}^k \geq 1 = 1 \quad (3)$$

$$DIXSG(cROT_{(level)})_{m,n}^k < 1 = 0 \quad (4)$$

Lastly, this study employs five sensitivity levels (50, 100, 150, 200, and 250) to compute the DIXSG within specific regions:

$$DIXSG_{(5-level)} = \frac{\sum_{L=1}^5 DIXSG\left(\left(cROT_{(level)}(L)\right)\right)}{N} \quad (5)$$

where  $L$  denotes the number of sensitivity levels. The position of each DIXSG is represented by the central point of each IPP pair, and the maximum value of  $DIXSG_{(5-level)}$  in a  $1^\circ \times 1^\circ$  or  $0.5^\circ \times 1^\circ$  area is chosen to represent the corresponding portion of the ionosphere at a given time (usually 1 hour).  $N$  represents the total count of valid areas, indicating the presence of at least one value within the area.

### 2.3 Rate of Total Electron Content Index (ROTI)

The ROTI introduced by Pi et al. (1997), serves as a metric for assessing ionospheric scintillation and irregularity based on GPS dual-frequency phase observations. ROTI is calculated as the standard deviation of the TEC rate (ROT) within a sliding window of 5 minutes (10 epochs) using GPS data sampled at a frequency of 30 seconds. To mitigate multipath effects, the elevation angle is typically set at  $30^\circ$ . The specific formula for ROTI calculation is as follows:

$$ROTI = \sqrt{\langle ROT^2 \rangle - \langle ROT \rangle^2} \quad (6)$$

where  $\langle \cdot \rangle$  denotes the time average within the sliding window,  $ROT$  represents the temporal derivative of Slant Total Electron Content (STEC) between two consecutive epochs. The  $ROT$  value is computed using the following equation:

$$ROT = \frac{STEC(i) - STEC(i-1)}{\Delta t} \quad (7)$$

where  $\Delta t$  represents the time interval between adjacent epochs in minutes, and  $i$  denotes the epoch. The STEC is determined using the formula as follows:

$$STEC(i) = \frac{\Phi_{L_1}(i) - \Phi_{L_2}(i)}{40.309 \cdot 10^{16} \cdot \left(\frac{1}{f_2^2} - \frac{1}{f_1^2}\right)} \quad (8)$$

where  $\Phi_{L_1}$  and  $\Phi_{L_2}$  refer to the carrier phase observations in the  $L_1$  and  $L_2$  frequency bands, while  $f_1$  and  $f_2$  represent the frequencies in the  $L_1$  and  $L_2$  bands, respectively, with  $f_1 = 1575.42$  MHz and  $f_2 = 1227.60$  MHz.

Small-scale plasma irregularities can have a significant impact on GPS signals, resulting in scintillation effects. In this analysis, ROTI is utilized to quantify the level of ionospheric plasma density irregularities and their influence on kinematic PPP solutions throughout the study (Yang et al., 2020). Assuming a thin-shell structure at an altitude of 350 km in the ionosphere, ROTI values are subsequently mapped to the corresponding IPPs (Nie et al., 2022).

### 2.4 GPS kinematic PPP solution

Kinematic PPP processing for carrier phase and pseudorange measurements was performed using the RTKLIB software (Real-Time Kinematic Library). The solution was computed with a sampling rate of 30 seconds. To mitigate the impact of multipath and ensure a sufficient number of satellites for accurate positioning, an elevation mask angle of  $10^\circ$  was applied.

To achieve high-precision results in kinematic PPP, error corrections were implemented for GPS dual-frequency observations. These corrections involved various sources of errors, including satellite-related factors such as clock offsets, orbit deviations, antenna phase offsets, and relativistic effects. Additionally, corrections were made for atmospheric errors, including ionospheric and tropospheric effects, as well as receiver-related errors such as clock offsets and antenna phase center deviations. Geophysical factors like tides and Earth rotation were also taken into account during the error correction process. Table 1 describes the settings.

## 3. Experimental results

### 3.1 Geomagnetic storm event description

On February 26th, a geomagnetic storm event occurred on Earth, which was influenced by a coronal mass ejection (CME) and a high-speed solar wind stream on February 24-25th, 2023. This geomagnetic storm had a prolonged duration and a significant level of disturbance, leading to ionospheric scintillation and a reduction in GPS positioning accuracy.

To evaluate the extent of disturbance caused by this geomagnetic storm, three indices, namely SYM-H, Kp, and ASY-H, were utilized to characterize the event. The SYM-H index (horizontal component asymmetry index) is computed every minute and can be regarded as a high-resolution Dst index (disturbance storm time index) (Wanliss & Showalter, 2006). The Dst index is classified into five levels: minor (-50, 30], moderate (-100, -50], strong (-200, -100], severe (-300, -200], and extreme ( $-\infty$ , -300]. The

Kp index (three-hourly geomagnetic index) is also divided into five levels: minor (5-, 5, 5+), moderate (6-, 6, 6+), strong (7-, 7, 7+), severe (8-, 8, 8-, 9-), and extreme (9<sub>0</sub>). The ASY-H index (vertical component

asymmetry index) is commonly employed to depict the activity level of auroras and exhibits a strong correlation with the trend of the AE index.

**Table 1.** Kinematic PPP Processing Strategy for GPS Dual-Frequency Ionosphere-Free Combinations

Parameters	Model and Strategy
Observations	GPS dual-frequency phase measurements
Processing model	Forward filtering
Cut off angle	10°
Sampling interval	30s
Cycle slip detection	GF and MW detection (TurboEdit)
Satellite orbit	IGS final precise orbits with a sampling interval of 15min
Satellite clock	IGS final clock products with a sampling interval of 30s
Phase center offset	igs08.atx
Ionospheric delay	Ionosphere-free model
Tropospheric delay	ZTD estimation
Differential Code Bias	Chinese Academy of Sciences rapid correction product
Solid earth tide	Model correction
Relativistic effects	Model correction
Earth Rotation	Earth rotation parameters provided by IGS

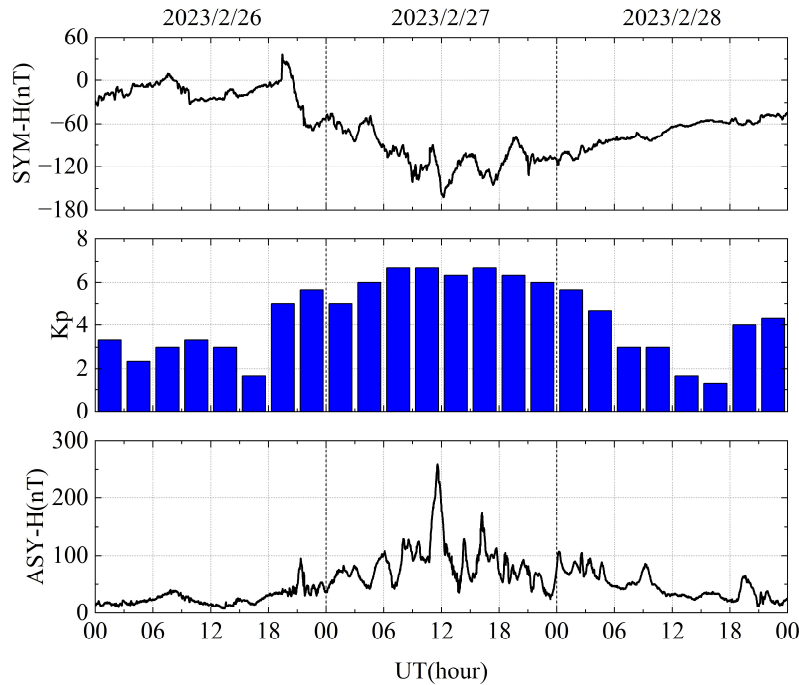


**Figure 2.** Geomagnetic index from February 26-28th, 2023.

Figure 2 illustrates the geomagnetic indices, SYM-H and Kp, during the period from February 26-28th, 2023. The ASY-H index is used as a substitute for the AE index. The SYM-H index was slightly elevated during the initial phase of the geomagnetic storm from 18:30 to 19:30 on February 26, followed by the main phase of the geomagnetic storm from 19:30 on February 26 to 21:00 on February 27, and

then finally the recovery phase, which recovered for a few days before returning to the normal level. The storm reached its peak at 12:00 on the 27th, with the minimum value of SYM-H reaching -161nT and the Kp index peaking at 6.67. This event can be categorized as a strong geomagnetic storm.

Figures 3, 4, and 5 present the Dst index for the

period of February 26-28, 2023, along with the DIXSG indices for three regions: Alaska, Canada, and Hong Kong. The DIXSG index is computed using the  $\Delta s$  weighting factor, which is larger at lower elevation angles and gradually decreases as the elevation angles increase. The figures demonstrate a strong correlation between the DIXSG index and the Dst index. However, as a regional index, the DIXSG index is expected to offer a more accurate reflection of the geomagnetic storm level in the specific region compared to the

global Dst index. By examining the DIXSG index, it is apparent that Alaska reached a peak state between 0:00 and 20:00 on the 27th, Hong Kong experienced peak periods from 10:00 to 15:00 and from 21:00 on the 27th to 3:00 on the 28th, while Canada did not exhibit a distinct peak in the DIXSG index. The subsequent sections will provide a detailed description of the relationship between the DIXSG index and positioning accuracy.

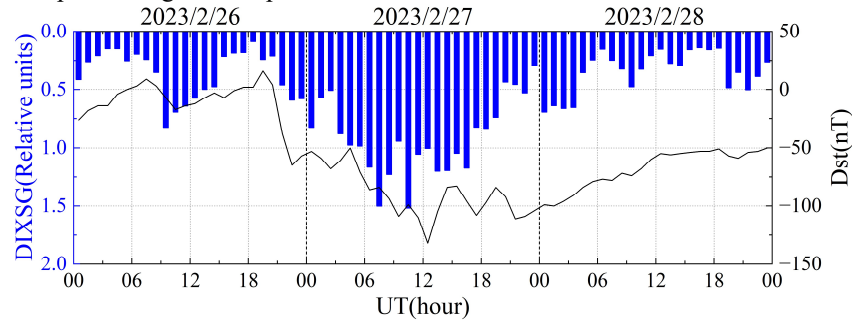


**Figure 3.** DIXSG index (blue) and Dst index (black) in Alaska from February 26-28th, 2023.

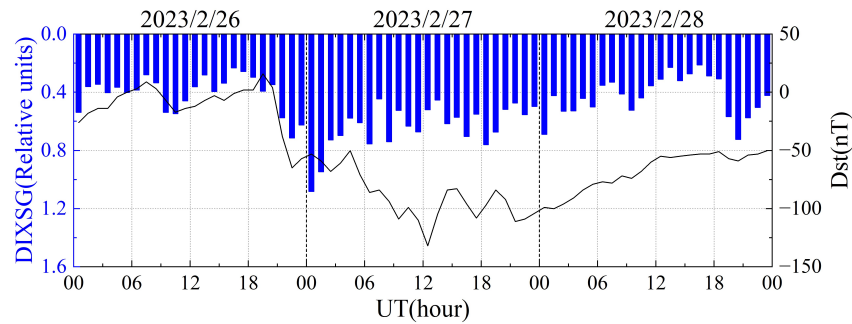


**Figure 4.** DIXSG index (blue) and Dst index (black) in CHAIN from February 26-28th, 2023.

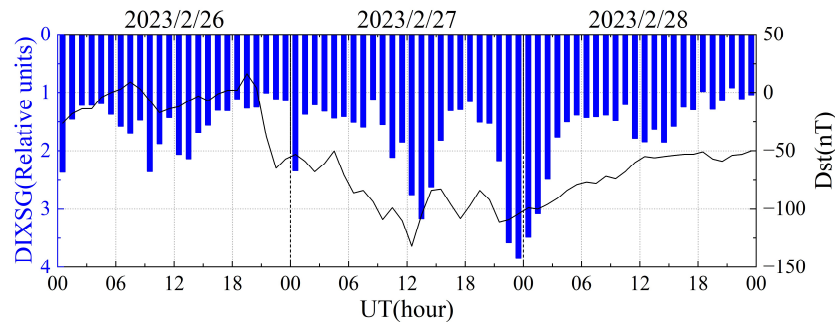


**Figure 5.** DIXSG index (blue) and Dst index (black) in Hong Kong from February 26 -28, 2023.

### 3.2 Analysis of the impact of global ionospheric scintillation on kinematic PPP errors

Figures 6 and 7 depict spatiotemporal maps with a 4-hour resolution, illustrating the variations in the ROTI and kinematic PPP errors for all stations between 18:00 on February 26th and 14:00 on February 28th, 2023. The blue shading represents nighttime, while the solid black line represents the magnetic equator. The IGS stations are denoted by

circles, Alaska stations by diamonds, CHAIN stations by stars, and Hong Kong Observation Network stations by pentagons. Analyzing the figures, it is evident that before the occurrence of the geomagnetic storm at 18:00 on the 26th, the ionosphere, as indicated by ROTI, was predominantly calm. With a few exceptions, the positioning accuracy remained within 0.1m. Notably, ionospheric scintillation occurred near the magnetic equator, resulting in decreased positioning accuracy of two stations in that region,

exceeding 0.5m and lasting for a certain duration. This phenomenon aligns with the characteristics of Equatorial Plasma Irregularities (EPI) after sunset (Wan et al., 2021). At 19:30, the geomagnetic storm entered its initial phase, causing disruptions of varying types, degrees, and geographical locations in the ionosphere due to geomagnetic activity. By 22:00, the storm phase was in effect. In high-latitude regions of North America, ROTI values were absent due to a 30° elevation cutoff angle setting. This was a consequence of poor observation quality at the time, resulting in fewer available observations for ROTI calculations. However, ionospheric scintillation persisted in this area, and the positioning accuracy of North American stations deteriorated significantly, with positioning errors mostly exceeding 0.5m. In low-latitude regions, positioning errors for several stations ranged from 0.15m to 0.30m. From 22:00 on February 26th to 6:00 on February 28th, the primary mid-to-high-latitude regions (40°-90°) and low-latitude regions near the magnetic equator were subject to the influence of the geomagnetic storm (Basu et al., 2002). By 14:00 on the 28th, the recovery phase of the geomagnetic storm had commenced, and the ionosphere reached a relatively calm state. Only a few stations were affected, and the positioning accuracy had returned to a centimeter-level accuracy.

The 4-hour resolution spatiotemporal maps provide an overview of the general characteristics and trends in ionospheric behavior and positioning impact during the geomagnetic storm. However, they cannot capture specific details. To address this limitation, this study generated dynamic maps with a 10-minute resolution. S1 ([i.postimg.cc/RVbMMYgN/S1.gif](https://i.postimg.cc/RVbMMYgN/S1.gif)) illustrates the global spatiotemporal variations of the ROTI, while S2 ([i.postimg.cc/VsgfhvM9/S2.gif](https://i.postimg.cc/VsgfhvM9/S2.gif)) displays the global spatiotemporal variations of PPP errors. Analysis of S1 and S2 reveals that the geomagnetic storm primarily influenced the ionosphere and positioning in the northern hemisphere. Through the geomagnetic storm event, the ionosphere and positioning accuracy in Antarctica and North America (40-90°) consistently experienced the effects. Numerous stations encountered compromised positioning accuracy, which can be attributed to the expansion of the auroral oval following intensified particle precipitation in regions with strong ionospheric irregularities. This phenomenon had a significant impact on positioning accuracy (Yang, et al., 2020). In contrast, the ionospheric scintillation

caused by the storm was less prominent in low-latitude regions. During the geomagnetic storm, ionospheric scintillation and the decrease in kinematic PPP accuracy occurred simultaneously, albeit with varying degrees of impact at different times during the storm. Detailed explanations will be provided based on the 10-minute resolution spatiotemporal maps of ROTI and PPP 3D RMS.

Starting from 20:00 on the 26th, ionospheric scintillation began to spread from high latitudes to mid-latitudes in North America, accompanied by an increase in the number of stations exhibiting positioning errors exceeding 0.5m. Between 22:00 on the 26th and 7:00 on the 27th, ionospheric scintillation and deteriorated positioning accuracy were observed near the geomagnetic equator. Scintillation near the geomagnetic equator and in low-latitude and mid-latitude regions predominantly occurred during the night and gradually subsided as the night progressed (Veellil et al., 2020). From 20:00 on the 26th to 7:00 on the 27th, the geomagnetic storm primarily impacted the geomagnetic equator and the Northern Hemisphere, displaying a trend of spreading from high latitudes to low latitudes. This trend can be attributed to Joule heating in high-latitude regions, which elevates the temperature of the upper atmosphere and drives the extension of the ionospheric storm from high to mid-low latitudes (Fuller-Rowell et al., 1994).

Between 7:00 and 9:30, the ionosphere near the geomagnetic equator and the positioning accuracy of stations returned to normal levels. During the peak moment of the geomagnetic storm (11:00 to 15:00), significant ionospheric scintillation occurred in Antarctica, above North America (40-90°), Hong Kong and its vicinity, Europe, and the eastern part of Australia. Between 11:00 and 13:00, over 80% of the stations above North America experienced positioning errors exceeding 0.5m, with the degradation of positioning accuracy lasting longer in the Hong Kong area. After the mitigation of ionospheric scintillation in the Hong Kong area, the North American region remained under the influence of the geomagnetic storm for an extended period, while other regions remained relatively calm until 20:00 on the 27th when another episode of ionospheric scintillation occurred in the vicinity of Hong Kong. This continued until 4:00 on the 28th. Between 22:00 on the 27th and 4:00 on the 28th, positioning accuracy in the Hong Kong area and its neighboring stations deteriorated.

## Global ROTI Maps

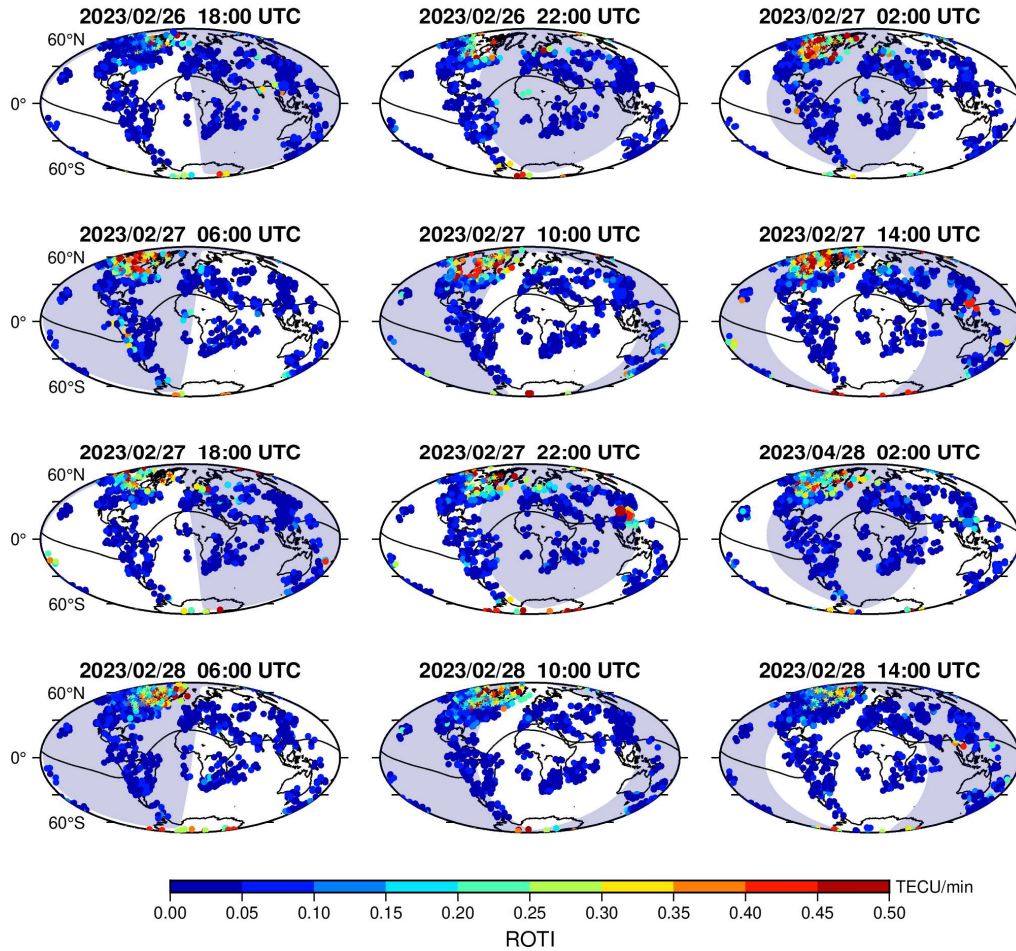


**Figure 6.** The global variations of ROTI from February 26th, 18:00 to February 28th, 14:00, with a resolution of 4 hours. The blue shading represents nighttime, while the solid black line represents the geomagnetic equator. Circles denote IGS stations, diamonds represent Alaska stations, stars represent the CHAIN observation network, and pentagons represent the Hong Kong observation network.

From 6:00 to 7:00 on the 28th, most global stations achieved normal centimeter-level positioning accuracy. However, after 7:00, some North American stations began to experience degradation in positioning accuracy. By 10:30 on the 28th, ROTI values had significantly decreased, and ROTI values in the high-latitude regions of the Northern Hemisphere were mostly within the normal range of 0.2-0.3. This phenomenon can be explained by complex particle precipitation in high-latitude regions (Juan et al., 2018). Although there were still mild scintillations, the positioning accuracy for most stations worldwide (excluding a few CHAIN stations in North America) had returned to normal levels. The geomagnetic storm was in the recovery phase, with

minimal impact on the ionosphere and positioning accuracy, indicating the return to normal geomagnetic activity levels and subsequent recovery of the ionosphere and positioning accuracy.

Ionospheric scintillation causes a degradation in positioning accuracy for numerous reasons. Ionospheric scintillation has a strong effect on the signal-to-noise ratio (SNR) of GPS signals, which can lead to cycle slips, satellite signal loss of lock, and degradation of PPP accuracy (Lu et al., 2020). Nie et al. (2022) found that the degradation of GPS observation quality (increase in carrier phase residuals) during the scintillation period also is one of the reasons for the decrease in positioning accuracy.

## Global PPP error Maps

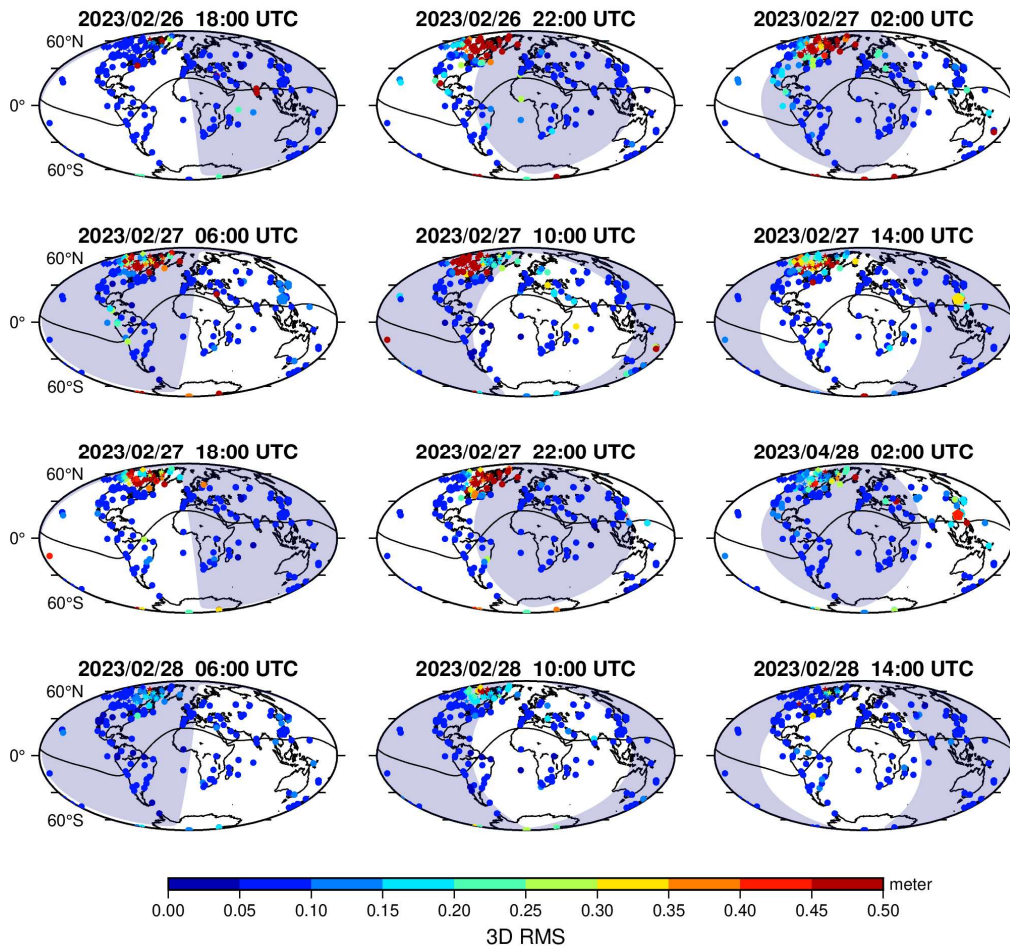


**Figure 7.** The global variations of 3D RMS error in kinematic PPP worldwide from February 26th, 18:00, to February 28th, 14:00, with a resolution of 4 hours. The blue shading indicates nighttime, while the solid black line represents the geomagnetic equator. IGS stations are represented by circles, Alaska stations by diamonds, the CHAIN observation network by stars, and the Hong Kong observation network by pentagons.

### 3.3 Analysis of the impact of regional geomagnetic storm on ionospheric scintillation and kinematic PPP errors

In Alaska, the DIXSG index peaked from 0:00 to 20:00 on the 27th (Figure 3). During this period, ionospheric scintillation was observed in the Alaska region (S1), and the station's positioning accuracy was suboptimal, with most stations experiencing positioning errors exceeding 0.5m (S2). Additionally, ROTI indicated the occurrence of ionospheric scintillation in Alaska from 22:00 on the 27th to 3:00 on the 28th (during the second scintillation period in the Hong Kong region). However, unlike the previous case, this ionospheric scintillation did not affect positioning accuracy.

From S1, it can be observed that ionospheric scintillation occurred in the Hong Kong region during two periods: 11:00 to 15:00 on the 27th and 20:00 on the 27th to 4:00 on the 28th. The DIXSG index in Figure 5 also reflects a peak period in the Hong Kong

region during the geomagnetic storm. Not only do the 18 stations in the Hong Kong observing network show an increase in ROTI and a decrease in positioning accuracy, but also several nearby stations show similar behavior. Due to the proximity of the Hong Kong stations, their characteristics cannot be observed on a global map. Therefore, separate spatio-temporal maps of kinematic PPP errors with a 1-hour resolution (Figure 8 and Figure 9) and positioning errors with a 10-minute resolution in the Hong Kong region (S3) (<https://i.postimg.cc/OQ4t68m6/S3.gif>) were generated. From Figure 8, Figure 9, and S3, it is evident that the first scintillation event in Hong Kong was significantly more severe than the second event. At its peak, the positioning accuracy of all 18 stations deteriorated to over 0.5m. As the 18 stations are closely located, the impact of the geomagnetic storm on their positioning is similar. It can be inferred that the influence of the geomagnetic storm on ionospheric scintillation and positioning accuracy is regional and affects a specific range.

For the CHAIN stations, it can be observed from S1 and S2 that they experienced the most severe impact on the ionosphere and positioning accuracy. Even at 14:00 on the 28th, when the positioning accuracy of most stations had returned to normal levels, several CHAIN stations still had positioning errors exceeding 0.5m. However, the DIXSG index in this region did not exhibit a clear peak and had

relatively small values. The reason for this could be that ionospheric scintillation in this area is not solely caused by the geomagnetic storm but rather by the interaction of charged particles in the auroral oval region descending along the Earth's magnetic field into the polar region atmosphere and colliding with atoms and molecules in the upper atmosphere, resulting in coupling effects with the ionosphere.

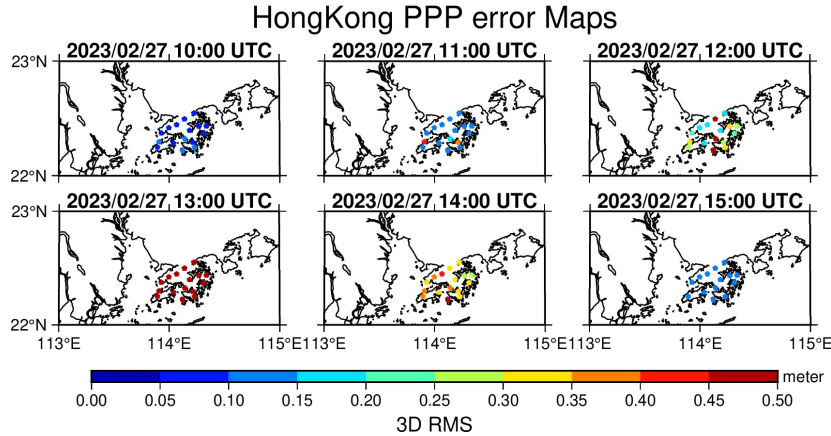


**Figure 8.** Global PPP 3D RMS variations maps from 10:00 to 15:00 on February 27, 2023 (1-hour resolution).

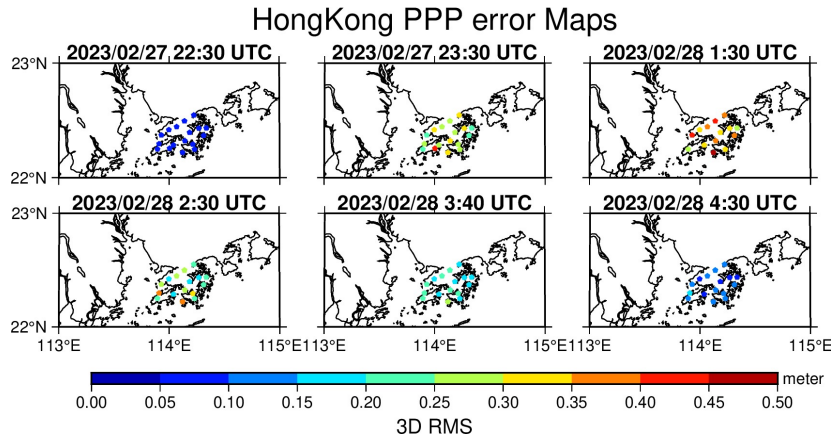


**Figure 9.** Global PPP 3D RMS variations maps from 22:30 on February 27, 2023, to 4:30 on February 28, 2023 (1-hour resolution). Since the PPP is the convergence time at 0:30 on the 28th, it is skipped.

#### 4 Conclusion

This study investigated the effects of ionospheric scintillation caused by a geomagnetic storm on kinematic PPP GPS positioning. Global IGS stations and three regional stations were analyzed for the period from February 26-28th, 2023. ROTI and DIXSG indices were utilized to assess the irregularities in plasma density induced by the storm. The findings highlight the following key points:

(1) Geomagnetic storms induce ionospheric scintillation, leading to degradation in positioning accuracy and potential loss of lock. However, it should be noted that not all ionospheric scintillation is directly linked to geomagnetic storms. Scintillation observed in the Canadian region, for example, is attributed to the interaction between charged particles and the

ionosphere. During intense geomagnetic storms, ROTI values indicate heightened levels of ionospheric scintillation, resulting in positioning errors exceeding 0.5m for the majority of stations.

(2) The impact of geomagnetic storms is significantly more pronounced in the Northern Hemisphere compared to the Southern Hemisphere, with North America (40-90°) experiencing particularly severe effects. Ionospheric scintillation typically initiates in high-latitude regions of North America and propagates towards lower latitudes. During the recovery phase of a geomagnetic storm, high-latitude stations are the last to regain normal positioning accuracy.

(3) Geomagnetic storms predominantly affect high-latitude and equatorial regions in terms of ionospheric scintillation and positioning accuracy.

Among these regions, high-latitude areas endure more severe consequences, including a higher number of affected stations, larger positioning errors, and longer durations of impact. In high-latitude regions, positioning errors frequently exceed 0.5m, while in equatorial regions, errors range from 0.15m to 0.5m.

(4) The DIXSG index exhibits a correlation with the Dst index, indicating the occurrence of geomagnetic storms and ionospheric scintillation. During the degradation phase of positioning accuracy in Hong Kong and Alaska stations, the DIXSG index reaches its peak.

(5) The impact of geomagnetic storms demonstrates regional characteristics, with stations within a specific region experiencing comparable levels of influence on positioning accuracy.

### Data Acquisition

SYM-H, Kp, ASY-H, and Dst data were obtained from the World Data Center for Geomagnetism, Kyoto ([wdc.kugi.kyoto-u.ac.jp/](http://wdc.kugi.kyoto-u.ac.jp/)). IGS station data were acquired from the National Aeronautics and Space Administration ([cdis.nasa.gov/](http://cdis.nasa.gov/)). Alaska station data were sourced from the Earth Scope Consortium ([observablehq.com/](http://observablehq.com/)). CHAIN station data were obtained from the Canadian High Arctic Ionospheric Network ([chain.physics.unb.ca/](http://chain.physics.unb.ca/)). Hong Kong data were collected from the Hong Kong Geodetic Survey Services ([www.geodetic.gov.hk/](http://www.geodetic.gov.hk/)).

### Acknowledgments

This research was supported by National Natural Science Foundation of China (Nos. 42204016, 42274021), the Natural Science Foundation of Jiangsu Province (No. BK20200664), State Key Laboratory of Geo-Information Engineering (No. SKLGIE2021-M-2-1), Key Laboratory of Polar Environment Monitoring and Public Governance (Wuhan University), Ministry of Education (No. 202305), Key Laboratory of Geospace Environment and Geodesy, Ministry of Education, Wuhan University (No. 20-01-09), Fundamental Research Funds for the Central Universities (No. 2020CXNL08), the China Postdoctoral Science Foundation (No. 2023M743762), the National Space Science Data Center (No. NSSDC2302003), the Construction Program of Space-Air-Ground-Well Cooperative Awareness Spatial Information Project (No. B20046), the Independent Innovation Project of “Double-First Class” Construction (No. 2022ZZCX06), and 2022 Jiangsu Provincial Science and Technology Initiative-Special Fund for International Science and Technology Cooperation (No. BZ2022018).

### References

Astafyeva, E.; Y. Yasyukevich; A. Maksikov and I. Zhivetiev (2014): Geomagnetic storms, super-

storms, and their impacts on GPS-based navigation systems. *Space Weather* 12(7):508–525.

Basu, S.; Sa Basu; CE Valladares; et al (2001): Ionospheric effects of major magnetic storms during the International Space Weather Period of September and October 1999: GPS observations, VHF/UHF scintillations, and in situ density structures at middle and equatorial latitudes. *Journal of Geophysical Research* 106(A12):30389–30413.

Basu, S.; KM Groves; et al (2002): Specification and forecasting of scintillations in communication navigation links: current status and future plans. *Journal of Atmospheric and Solar-Terrestrial Physics* 64(16):1745-1754.

Basu, S and KM Groves (2002): Specification and Forecasting of Outages on Satellite Communication and Navigation Systems. *Geophysical Monograph Series* 125:423-430.

Bergeot, N.; C. Bruyninx et al (2011): Impact of the Halloween 2003 ionospheric storm on kinematic GPS positioning in Europe. *GPS Solutions* 15(2):171–180.

Béniguel, Y.; JP Adam; A. Bourdillon and P. Lassudrie-Duchesne (2011): Ionosphere scintillation effects on navigation systems. *Comptes Rendus Physique* 12(2):186–191.

Conker, RS; MB El-Arini; CJ Hegarty and T. Hsiao (2003): Modeling the effects of ionospheric scintillation on GPS/Satellite-based augmentation system availability. *Radio Science* 38(1):1–23.

Fuller-Rowell, TJ; MV Codrescu; RJ Moffett and S. Quegan (1994): Response of the thermosphere and ionosphere to geomagnetic storms. *Journal of Geophysical Research* 99(A3): 3893–3914.

Gonzalez WD; JA Joselyn et al (1994): What is a geomagnetic storm? *Journal of Geophysical Research* 99 (A4):5771– 5792.

Jakowski N.; S. Stankov; S. Schlueter and D. Klaehn (2006): On developing a new ionospheric perturbation index for space weather operations. *Advances in Space Research* 38(11): 2596–2600.

Jakowski N.; C. Borries and V. Wilken (2012): Introducing a disturbance ionosphere index. *Radio Science* 47(4): RS0L14.

Jiao Y and YT Morton (2015): Comparison of the effect of high-latitude and equatorial ionospheric scintillation on GPS signals during the maximum of solar cycle 24. *Radio Science* 50(9):886– 903.

Juan JM; J. Sanz; et al (2018): AATR an ionospheric activity indicator specifically based on GNSS measurements. *Journal of Space Weather and Space Climate* 8(A14):11.

Li G.; B. Ning; Z. Ren and L. Hu (2010): Statistics of GPS ionospheric scintillation and irregularities

- over polar regions at solar minimum. *GPS Solutions* 14(4):331–341.
- Lu Y.; Z. Wang; S. Ji and W. Chen (2020): Assessing the Positioning Performance Under the Effects of Strong Ionospheric Anomalies with Multi-GNSS in Hong Kong. *Radio Science* 55(8): e2019RS007004.
- Luo X.; Y. Lou, Q. Xiao; S. Gu; B. Chen and Z. Liu (2018): Investigation of ionospheric scintillation effects on BDS precise point positioning at low-latitude regions. *GPS Solutions* 22(3): 63.
- Luo X.; J. Du; et al (2022): A method to mitigate the effects of strong geomagnetic storm on GNSS precise point positioning. *Space Weather* 20(1): e2021SW002908.
- Mansilla GA (2019): Behavior of the Total Electron Content over the Arctic and Antarctic sectors during several intense geomagnetic storms. *Geodesy and Geodynamics* 10(1):26-36.
- Marques, HAS; JFG Monico and HA Marques (2016): Performance of the L2C civil GPS signal under various ionospheric scintillation effects. *GPS Solutions* 20(2):139–149.
- Nava, B.; J. Rodríguez-Zuluaga; et al (2016): Middle- and low-latitude ionosphere response to 2015 St. Patrick's Day geomagnetic storm. *Journal of Geophysical Research: Space Physics* 121(4):3421–3438.
- Nie, W.; A. Rovira-Garcia; et al (2022): On the global kinematic positioning variations during the September 2017 solar flare events. *Journal of Geophysical Research: Space Physics* 127(8): e2021JA030245.
- Odijk, D. (2001): Instantaneous Precise GPS Positioning under Geomagnetic Storm Conditions. *GPS Solutions* 5(2):29–42.
- Pi, X.; A. Mannucci; U. Lindqwister and C. Ho (1997): Monitoring of global ionospheric irregularities using the worldwide GPS network. *Geophysical Research Letters* 24(18):2283–2286.
- Vadakke, Veetil S.; M. Aquino; Ham Marques and A. Moraes (2020): Mitigation of ionospheric scintillation effects on GNSS precise point positioning (PPP) at low latitudes. *Journal of Geodesy* 94(2):15.
- Wanliss, JA and KM Showalter (2006): High-resolution global storm index: Dst versus SYM-H. *Journal of Geophysical Research* 111(A2): A02202.
- Wan, X.; C. Xiong; et al (2021): The nighttime ionospheric response and occurrence of equatorial plasma irregularities during geomagnetic storms: a case study. *Satellite Navigation* 2(1):23.
- Wilken, V.; M. Krieger; N. Jakowski and J. Berdermann (2018): An ionospheric index suitable for estimating the degree of ionospheric perturbations, *Journal of Space Weather and Space Climate* 8(A19):9.
- Yang, Z.; Y TJ Morton; I. Zakharenkova; I. Cherniak; S. Song and W. Li (2020): Global view of ionospheric disturbance impacts on kinematic GPS positioning solutions during the 2015 St. Patrick's Day storm. *Journal Of Geophysical Research: Space Physics* 125(7): e2019JA027681.
- Zhang, X.; F. Guo and P. Zhou (2014): Improved precise point positioning in the presence of ionospheric scintillation. *GPS Solutions* 18(1):51–60.
- Zhao, D.; CM Hancock; GW Roberts and S. Jin (2019): Cycle Slip Detection during High Ionospheric Activities Based on Combined Triple-Frequency GNSS Signals. *Remote sensing* 11(3):250.
- Zhao, D.; L. Wang; et al (2022): Statistical Study on the Characterization of Phase and Amplitude Scintillation Events in the High-latitude Region During 2014-2020 Based on ISMR. *Advances in Space Research* 69(9):3435-3459.

## Authors



**Shuanglei Cui** is currently a master's student at China University of Mining and Technology. His research interest is GNSS positioning under ionospheric scintillation.



**Xueli Zhang** is currently a master's student at China University of Mining and Technology. His research interest is ionospheric scintillation monitoring.



**Dongsheng Zhao** is an associate professor at the School of Environment and Spatial Informatics, China University of Mining and Technology. He received his Ph.D. and B.Eng degrees from the University of Nottingham and Wuhan University, respectively. His current research interests focus on GNSS remote sensing, particularly in ionospheric scintillation monitoring and modeling.



**Wei Ban** is an associate professor at the Chinese Antarctic Center of Surveying and Mapping, Wuhan University. He received his Ph.D. degree from Wuhan University. His current research interests focus on GNSS remote sensing and applications.



**Qianxin Wang** is a Professor and the vice-dean at the School of Environment and Spatial Informatics, China University of Mining and Technology. He received his Ph.D. degree from Central South University, China. His current research interests include geodetic data processing and satellite positioning.



**Craig M. Hancock** is a Reader in surveying at the School of Architecture, Building and Civil Engineering, Loughborough University. He obtained his Ph.D. degree from Newcastle University and worked in the University of Nottingham for 14 years. His research interests are GNSS error source modeling, BIM and digital construction.



**Kefei Zhang** is a Professor at the School of Environment and Spatial Informatics, China University of Mining and Technology. He received his Ph.D. degree from Curtin University, Australia. His research interests include GNSS atmospheric modeling, space mining and precision agriculture.